NO Binding Induced Conformational Changes in a Truncated Hemoglobin from *Mycobacterium tuberculosis*[†]

Masahiro Mukai,[‡] Yannick Ouellet,[§] Hugues Ouellet,[§] Michel Guertin,[§] and Syun-Ru Yeh*,[‡]

Department of Physiology and Biophysics, Albert Einstein College of Medicine, Bronx, New York 10461, and Department of Biochemistry and Microbiology, Faculty of Sciences and Engineering, Laval University, Quebec G1K 7P4, Canada

Received October 4, 2003; Revised Manuscript Received December 23, 2003

ABSTRACT: The resonance Raman spectra of the NO-bound ferric derivatives of wild-type HbN and the B10 Tyr → Phe mutant of HbN, a hemoglobin from *Mycobacterium tuberculosis*, were examined with both Soret and UV excitation. The Fe−N−O stretching and bending modes of the NO derivative of the wild-type protein were tentatively assigned at 591 and 579 cm^{-1}, respectively. Upon B10 mutation, the Fe−NO stretching mode was slightly enhanced and the bending mode diminished in amplitude. In addition, the N−O stretching mode shifted from 1914 to 1908 cm^{-1}. These data suggest that the B10 Tyr forms an H-bond(s) with the heme-bound NO and causes it to bend in the wild-type protein. To further investigate the interaction between the B10 Tyr and the heme-bound NO, we examined the UV Raman spectrum of the B10 Tyr by subtracting the B10 mutant spectrum from the wild-type spectrum. It was found that, upon NO binding to the ferric protein, the Y_{8a} mode of the B10 Tyr shifted from 1616 to 1622 cm^{-1}, confirming a direct interaction between the B10 Tyr and the heme-bound NO. Furthermore, the Y_{8a} mode of the other two Tyr residues at positions 16 and 72 that are remote from the heme was also affected by NO binding, suggesting that NO binding to the distal site of the heme triggers a large-scale conformational change that propagates through the pre-F helix loop to the E and B helices. This large-scale conformational change triggered by NO binding may play an important role in regulating the ligand binding properties and/or the chemical reactivity of HbN.

Nitric oxide (NO) is a free radical with multiple and diverse biological functions (*1*−*5*). Interactions of NO with Fe-protoporphyrin in heme proteins are of great physiological importance (*1*). The ferric heme of nitrophorin, isolated from bloodsucking insects, binds NO strongly in the salivary glands (pH ∼5) and releases it in host tissues (pH ∼7) to induce local vasodilation to ensure a large blood flow, taking advantage of the pH-dependent NO binding affinity (*6*, *7*). The NO generated by nitric oxide synthase (NOS) geminately rebinds to the heme active site, resulting in reversible feedback inhibition for NO release (*8*−*13*). On the other hand, the binding of NO and the subsequent breakage of the proximal iron−histidine bond in the heme domain of soluble guanylate cyclase (sGC) induce allosteric structural changes in the catalytic domain, activating the conversion of GTP to cGMP (*9*, *10*, *14*). Despite its physiological importance, very little is known with regard to the structural transition triggered by NO binding to the heme in these proteins, which is essential for their functions.

For hemoglobin or myoglobin, the ferrous heme binds strongly to NO with a much higher affinity than CO and O_2 (*15*, *16*). The ferric protein also binds NO, but with a much lower affinity. In this work, we studied the NO adduct of ferric HbN, one of the two hemoglobins from *Mycobacterium tuberculosis* (*17*−*19*). HbN is a homodimeric protein. It belongs to the newly discovered truncated hemoglobin family, members of which are characterized by a novel two-over-two α-helical sandwich motif (*20*), the absence of the A helix, and the presence of an extended loop substituting for most of the F helix (Figure 1). Like mammalian globins, HbN binds various heme ligands reversibly (*18*, *19*). Resonance Raman studies suggest that these heme-bound ligands are stabilized by a distal Tyr residue at the B10 position (*18*), which has been subsequently confirmed by the recent crystallographic data (*20*). Biochemical and biophysical studies suggest that the oxygen affinity of HbN is extremely high and its biological function may be involved in NO detoxification (*18*, *19*, *21*).

Here we employed resonance Raman spectroscopy with both Soret and UV excitation to study the structural transition induced by NO binding to the wild type and the B10 Tyr → Phe mutant of the ferric derivative of HbN. Resonance Raman spectroscopy with Soret excitation has been successfully applied in studying structural and functional relationships of heme proteins for more than three decades (*22*). On the contrary, UV Raman spectroscopy has not been as widely utilized until more recently (*23*−*26*), because heme proteins are typically highly susceptible to UV photodamage and suitable commercial continuous-wave UV lasers were not available in the past. We employed resonance Raman spectroscopy with 406.7 and 244.0 nm excitation to inves-

[†] This work was supported by National Institutes of Health Grant HL65465 to S.-R.Y. and by Natural Sciences and Engineering Research Council of Canada Grant 06P0046306 to M.G.

* To whom correspondence should be addressed. Telephone: (718) 430-4234. Fax: (718) 430-4230. E-mail: syeh@aecom.yu.edu.

[‡] Albert Einstein College of Medicine.

[§] Laval University.

10.1021/bi035798o CCC: $27.50
Published on Web 00/00/0000 PAGE EST: 6.9

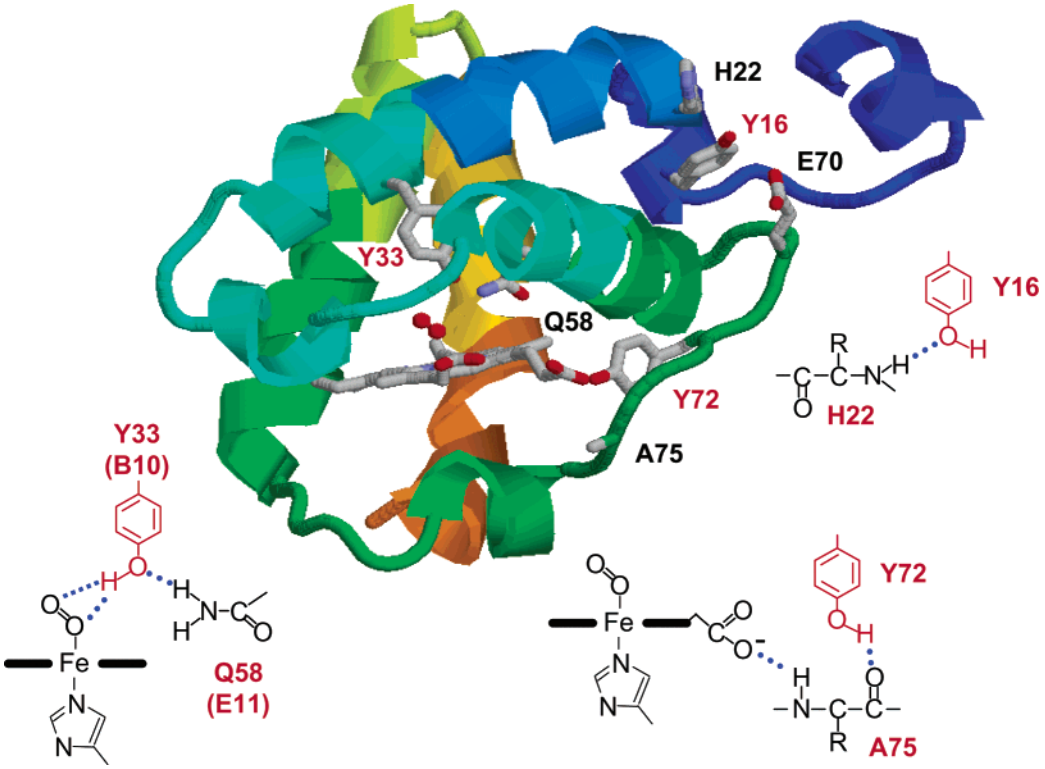

FIGURE 1: Crystal structure of subunit B of the oxy derivative of HbN (PDB entry 1IDR). HbN is a homodimer; but the two subunits, A and B, have slightly different structures. The insets illustrate the chemical environments of the three Tyr residues at positions 16, 33, and 72 based on subunit B.

tigate the structure of the Fe−NO moiety. In addition, the structural changes induced by NO binding to the heme distal pocket were explored by monitoring the vibrational modes of Tyr residues at positions 16, 33, and 72 that are located in N-terminal, the distal, and the proximal side of the heme, respectively. It has been shown that the vibrational modes of Tyr are very sensitive to the environment of its surroundings (*vide infra*). On the basis of the crystal structure of the oxy derivative, each of the three Tyr residues forms a unique and sophisticated H-bonding network with its surroundings as illustrated in Figure 1. The new data reported here demonstrate that the binding of NO to the heme iron triggers a large-scale structural change, which may play an important role in regulating the ligand binding properties and/or the chemical reactivity of HbN.

MATERIALS AND METHODS

Recombinant *M. tuberculosis* HbN was cloned, expressed, and purified to near homogeneity as described elsewhere (*18*, *19*). The single-amino acid substitution mutant of HbN (B10 Tyr → Phe) was prepared as described previously. The protein was buffered with 50 mM Tris at pH 7.5. $^{14}N^{16}O$ and $^{15}N^{16}O$ were purchased from Icon (Mt. Marion, NY).

The Raman measurements with Soret excitation were taken with previously described instrumentation (*18*, *19*). Briefly, the output at 406.7 nm from a krypton ion laser (Spectra Physics) was focused to a ~30 μm spot (laser power of ~2 mW) on a rotating cell to prevent photodamage to the sample. The scattered light was collected at right angles to the incident beam and focused on the entrance slit of a 1.25 m polychromator (Spex) where it was dispersed and then detected with a charge-coupled device (Princeton Instruments). The protein concentration used for the Soret excitation experiments was 50 μM. The acquisition time was ~30 min for each spectrum. All the Raman spectra with Soret excitation were calibrated with indene (Sigma). Optical absorption spectra were acquired before and after spectral acquisition to ensure that there is no photodamage occurring to the sample during the spectral acquisition.

For the UV Raman measurements, the output at 244.0 nm from a frequency-doubled Ar ion laser (Coherent Inc) was focused on a quartz spinning cell. To avoid photodamage to the sample, a small metal stirring ball, controlled by an external magnet, was introduced inside the solution compartment on the basis of the design reported by Aki *et al.* (*27*). In addition, the laser power was kept below 300 μW, and for every UV Raman spectrum, three independent spectral acquisitions, each with 10 min of accumulation with a freshly prepared sample, were obtained and averaged. The integrity of the samples was confirmed by UV−visible absorption measurements following each acquisition. The scattered light was collected at right angles to the incident beam and focused on the entrance slit of a 1 m polychromator (Spex), where it was dispersed and then detected with a charge-coupled device (Spex). All the UV Raman spectra were calibrated with a mixture of cyclohexane and trichloroethylene. Sodium perchlorate (0.03 M) was added to each sample solution as an internal standard for UV Raman measurements. The spectral contributions from the solvent and glass were subtracted from each UV Raman spectrum.

RESULTS

The NO-bound ferric HbN has a typical six-coordinate low-spin configuration based on the high-frequency resonance Raman spectrum (1300−1700 cm^{-1}) obtained with Soret excitation at 406.7 nm (data not shown). The corre-

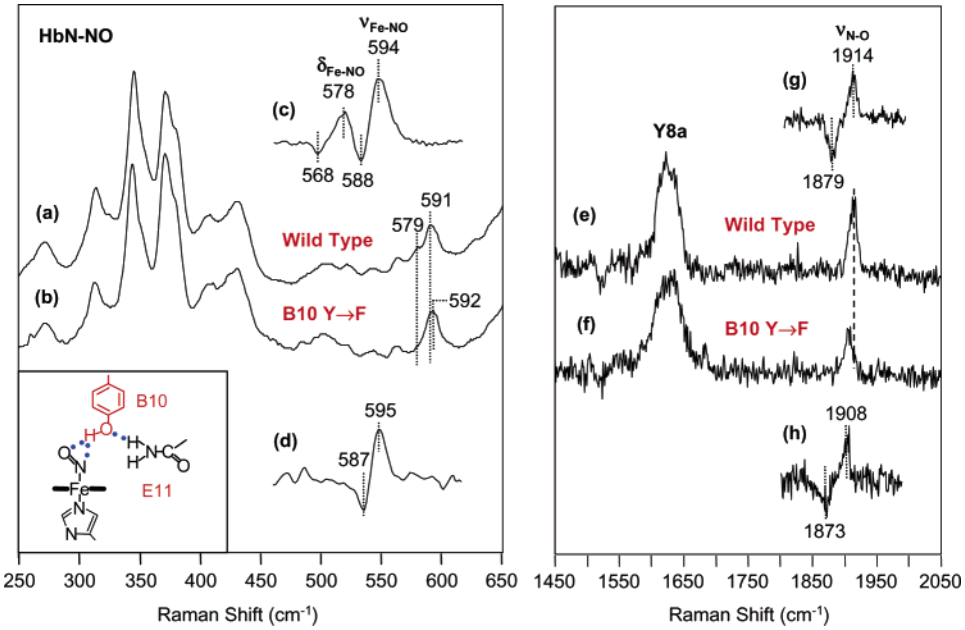

FIGURE 2: Raman spectra of the NO derivatives of the ferric HbN with Soret excitation at 407 nm (a−d) and UV excitation at 244 nm (e−g). The spectra of the wild-type protein are spectra a and e; those of the B10 Tyr → Phe mutant are spectra b and f. The $^{14}N^{16}O - {}^{15}N^{16}O$ isotope difference spectra of spectra a, b, e, and f are shown as spectra c, d, g, and h, respectively. The inset in the left panel shows the postulated H-bonding interaction between the heme-bound NO and B10 Tyr.

sponding low-frequency resonance Raman spectrum is shown in Figure 2a. The ν_{Fe-NO} and δ_{Fe-N-O} modes were tentatively assigned at 591 and 579 cm^{-1}, respectively, based on the $^{14}N^{16}O - {}^{15}N^{16}O$ isotope difference spectrum shown in Figure 2c, although firm assignments have to be confirmed with additional NO isotopic substitution experiments. Similar measurements were performed with the B10 Tyr → Phe mutant (Figure 2b,d). After the mutation is introduced, the δ_{Fe-N-O} bending mode is totally diminished in amplitude, but the ν_{Fe-NO} stretching frequency is almost the same as that in the wild-type protein.

The N−O stretching modes of NO-bound ferric heme proteins are difficult to observe with Soret excitation due to their weak Raman cross section. Recently, it was reported that this mode may be dramatically enhanced with UV excitation at 244 nm (*28*). For this, we measured the Raman spectrum of the NO-bound ferric protein with 244 nm excitation. Figure 2e shows the UV Raman spectrum of the NO-bound wild-type protein. The broad peak centered at 1619 cm^{-1} was assigned to the Y_{8a} vibrational mode from the Tyr residues (*vide infra*). The band at 1914 cm^{-1} was assigned to the N−O stretching mode based on its shift to 1879 cm^{-1} upon the $^{15}N^{16}O$ isotope substitution (Figure 2g). Similarly, the N−O stretching mode of the B10 Tyr → Phe mutant was identified at 1908 cm^{-1}. It shifted to 1873 cm^{-1} upon the $^{15}N^{16}O$ isotope substitution (Figure 2h). The lower frequency of the N−O stretching mode in the mutant protein suggests that the B10 Tyr forms an H-bond(s) with the heme-bound NO in the wild-type protein, which reduces the electron density in the π^* antibonding orbital of NO, and consequently strengthens the N−O bond. H-Bonding interactions were also observed in the O_2, CO, and aquo-met derivatives of HbN (*18*, *19*).

Despite the 6 cm^{-1} difference in the N−O stretching frequency with the mutation, no change was observed in the Fe−NO stretching frequency, suggesting that the Fe−N−O moiety in HbN is bent, because an inverse correlation between the Fe−NO and N−O bond strength would be expected otherwise, based on the following resonance structures of the Fe−N−O moiety.

$$\underset{\text{(I)}}{Fe{=}N{=}O} \leftrightarrow \underset{\text{(II)}}{Fe^{\delta-}{-}N{\equiv}O^{\delta+}} \qquad (1)$$

Similar conclusions have been drawn for the Fe−CO complexes of heme-containing proteins by Spiro *et al.* (*29*). Bent Fe^{3+}−NO complexes have been reported for P450 and chloroperoxidase due to steric and crowding effects imposed by bulky substrates (*30*, *31*). In addition, a bent Fe^{3+}−NO complex was recently discovered in the ferric derivative of nitrophorin (*32*), which was attributed to steric hindrance and protein-assisted heme ruffling (*33*). The disappearance of the Fe−N−O bending mode in the B10 Tyr → Phe mutant of HbN is consistent with the postulate that the Fe−NO moiety is bent in the wild-type protein, because the bending mode is typically enhanced for a bent structure. Taken together, the data suggest that the B10 Tyr in the wild-type protein forms an H-bond(s) with the heme-bound NO and causes the Fe−N−O moiety to be bent as illustrated in the inset in the left panel of Figure 2.

In addition to the N−O stretching mode, UV Raman spectroscopy with 244 nm excitation also provides useful information with regard to the vibrational modes of amino acid residues with conjugated double bonds, including Trp, Tyr, Phe, and His (*34*, *35*). In general, the UV Raman spectrum of protein molecules is dominated by the vibrational modes from Tyr and Trp, because the Raman cross sections of Phe and His are much weaker with 244 nm excitation. HbN does not have any Trp residues, but it has three Tyr residues at positions 16, 33, and 72. On the basis of the crystal structure of the oxy derivative, they are located in the N-terminal, the distal, and the proximal sides of the heme, respectively. Each Tyr residue form a tight H-bonding network with neighboring residues as illustrated in Figure 1.

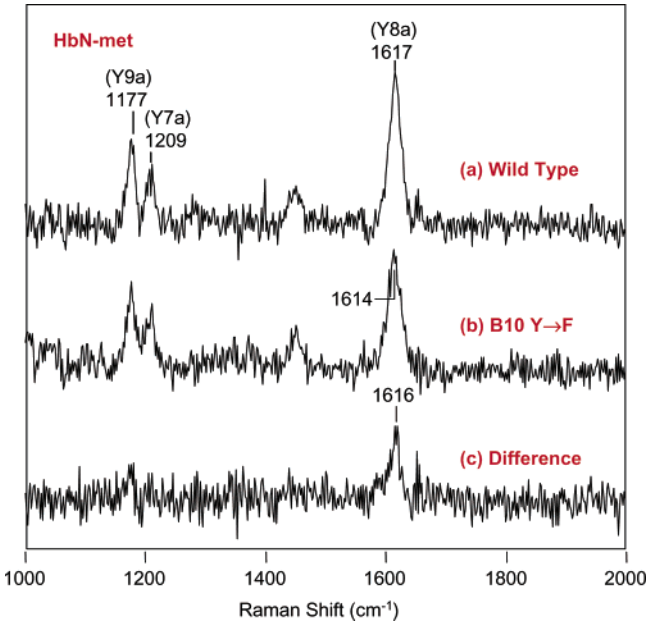

FIGURE 3: UV Raman spectra of the ferric (aquo-met) form of wild-type HbN (a) and the B10 Tyr → Phe mutant (b) with 244 nm excitation. Trace c is the difference spectrum between spectra a and b. Sodium perchlorate (0.03 M) was added to the protein solutions as an internal intensity standard for spectral subtraction.

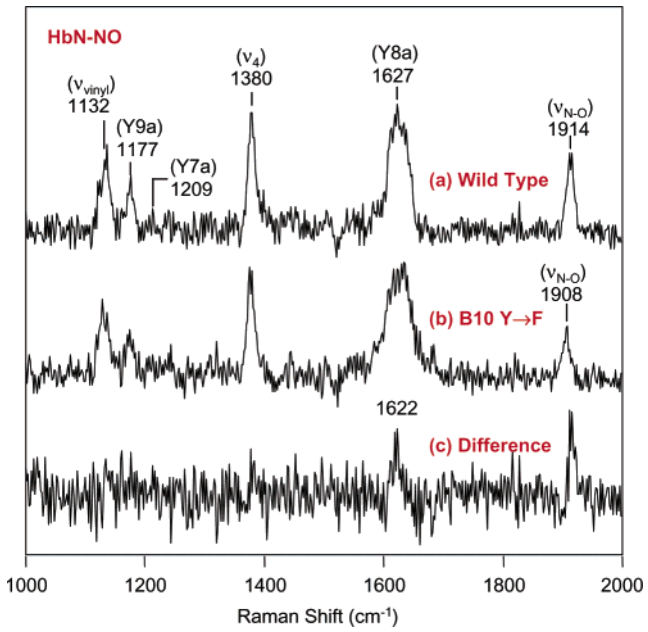

FIGURE 4: UV Raman spectra of the NO derivative of wild-type HbN (a) and the B10 Tyr → Phe mutant (b) with 244 nm excitation. Trace c is the difference spectrum between spectra a and b. Sodium perchlorate (0.03 M) was added to the protein solutions as an internal intensity standard for spectral subtraction.

Figures 3a and 4a show the UV Raman spectrum of the aquo-met and NO derivatives, respectively, of the ferric HbN in the 1000−2000 cm^{-1} region. In the aquo-met derivative, the vibration modes at 1617, 1209, and 1177 cm^{-1} were assigned to the Y_{8a}, Y_{7a}, and Y_{9a} modes of Tyr, respectively (*24*). When NO bound to the ferric protein, the Y_{8a} mode shifted to 1627 cm^{-1} (Figure 4a), and the bandwidth increased from 25 to 38 cm^{-1}, suggesting increased structural flexibility or heterogeneity. Furthermore, the intensity of the Y_{9a} mode is slightly reduced, although the peak position

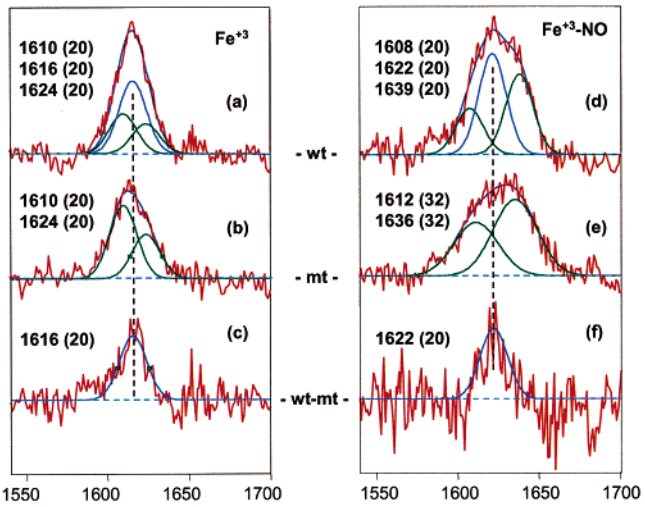

FIGURE 5: Spectral deconvolution of the Y_{8a} modes of the Tyr residues in the wild-type protein (a and d) and the B10 Tyr → Phe mutant protein (b and e). Traces c and f are a − b and d − e difference spectra, respectively. The original spectra were taken from Figures 3 and 4. The peak maxima and widths used for the fitting (the numbers in parentheses) are indicated in each spectrum.

remained unperturbed. On the other hand, the Y_{7a} mode is almost totally diminished in amplitude. In addition to these Tyr modes, three additional bands at 1914, 1380, and 1132 cm^{-1} were observed. The 1914 cm^{-1} band is assigned to the N−O stretching mode as discussed earlier. The 1380 cm^{-1} band is assigned to the ν_4 mode of the heme prosthetic group (*35*), and the 1132 cm^{-1} band is assigned to a vibrational mode involving motion of the vinyl group of the heme (*36*). Similar modes have been identified in the cyanide-bound ferric protein of horseradish peroxidase with 244 nm excitation (*35*). They are also observed in horse heart myoglobin as will be discussed below. The enhancement of these modes in the six-coordinate low-spin ferric proteins with 244 nm excitation suggests that the six-coordinate low-spin heme may have an electronic transition in the 244 nm region.

To investigate the environment of the B10 Tyr residue, we measured the resonance Raman spectrum of the B10 Tyr → Phe mutant. In the aquo-met form, the Y_{8a} mode shifted to a lower frequency at 1614 cm^{-1}, while the Y_{9a} and Y_{7a} modes were unaffected by the mutation as shown in Figure 3b. The Y_{8a} mode of the mutant can be deconvoluted into two Gaussian peaks with maxima at 1610 and 1624 cm^{-1} and a width of ∼20 cm^{-1}, as illustrated in Figure 5b, which were assigned to the two Tyr residues at positions 16 and 72, respectively, in this mutant protein. The UV resonance Raman spectrum of the single B10 Tyr33 could be obtained by subtracting the spectrum of the B10 Tyr → Phe mutant from that of the wild-type protein as shown in Figure 3c, assuming that the environments of Tyr16 and Tyr72 were not affected by the mutation of B10 Tyr33. On the basis of the difference spectrum, the Y_{8a} mode of the Tyr33 residue is centered at 1616 cm^{-1}. This peak can be fitted with a Gaussian function with a center at 1616 cm^{-1} and a width of ∼20 cm^{-1} as shown in Figure 5c. The frequency differences in the Y_{8a} modes of Tyr33, Tyr16, and Tyr72 suggest that the environment of each Tyr residue is distinct. To confirm these assignments, the Y_{8a} mode of the wild-type protein is deconvoluted into three Gaussian functions

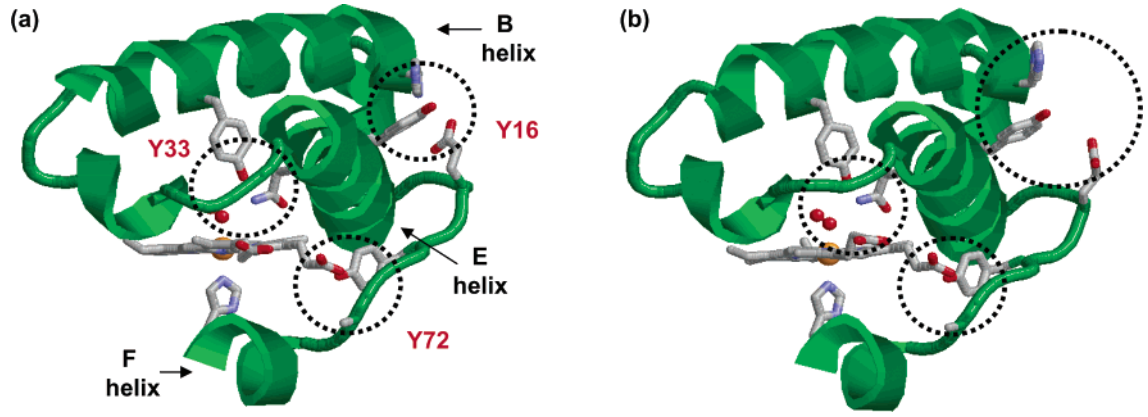

FIGURE 6: Structural differences between subunit A (a) and subunit B (b) of the homodimeric HbN (PDB entry 1IDR; only residues 15−81 are shown). The B, E, and F helices are labeled as indicated. The three Tyr residues at positions 16, 33, and 72, along with the residues that form H-bonds with these three residues, are presented in stick format.

by fixing the peak positions at 1610, 1616, and 1624 cm^{-1} with a width of 20 cm^{-1}. As shown in Figure 5a, the residual from the fitting is negligible and the intensity ratio between the 1610 and 1624 cm^{-1} peaks is almost identical to that of the mutant protein shown in Figure 5b. The successful reconstitution of the Y_{8a} mode of the wild-type protein with that of the mutant protein and that of the B10 Tyr suggests that the B10 Tyr → Phe mutation does not affect the environment of Tyr16 and Tyr72.

On the other hand, the Y_{8a} mode of the NO derivative slightly shifted to a higher frequency upon the B10 Tyr → Phe mutation, and the spectral width increased from 38 to 51 cm^{-1} (Figure 4a,b). The rest of the spectrum was not affected by the mutation, except that the N−O stretching mode shifted from 1914 to 1908 cm^{-1}, as a result of the direct interaction between B10 Tyr and NO as discussed earlier. The Y_{8a} mode of the mutant can be deconvoluted into two Gaussian functions with the centers at 1612 and 1636 cm^{-1} and a width of 32 cm^{-1} as shown in Figure 5e. These two peaks were assigned to Tyr16 and Tyr72, respectively. The Y_{8a} mode in the difference spectrum between the wild type and the mutant protein (Figure 4c) can be fitted with a Gaussian function with a center at 1622 cm^{-1} and a width of ∼20 cm^{-1} (Figure 5f). In contrast to the aquo-met derivative, the Y_{8a} mode of the wild-type protein cannot be reconstituted with the three Gaussian functions extracted from spectra e and f of Figure 5. Instead, it was deconvoluted into three new Gaussian functions with centers at 1608, 1622, and 1639 cm^{-1} and widths of ∼20 cm^{-1}. On the basis of spectra e and f of Figure 5, the 1622 cm^{-1} peak was assigned to B10 Tyr33, and the other two were assigned to Tyr16 and Tyr72. The 1608 cm^{-1} peak was tentatively assigned to the same origin as the 1612 cm^{-1} peak found in the mutant protein. Likewise, the 1639 cm^{-1} (Figure 5d) and 1636 cm^{-1} (Figure 5e) peaks were assigned to the same origin. The changes in the peak maxima of the Y_{8a} modes of the three Tyr residues in the NO derivative of the wild-type protein (Figure 5d) with respect to the aquo-met derivative (Figure 5a) suggest that NO binding to the heme iron causes dramatic structural changes in the protein moiety. On the other hand, the relatively broader peaks in the spectrum of the B10 Tyr → Phe mutant of the NO derivative (spectrum e vs spectrum d of Figure 5) suggest that the protein loses its rigidity upon mutation, which results in an increased conformational flexibility in the structural region near Tyr16 and Tyr72. A direct reaction between NO and the Tyr residues is excluded because the addition of NO to the phenyl ring would alter the symmetry of the molecule and thereby significantly perturb the vibrational modes of the Tyr residues.

DISCUSSION

To understand the Raman data in the context of the protein structure, we examined the crystal structure of the oxy derivative of HbN (PDB entry 1IDR), the only crystal structure available for HbN. HbN is a homodimer with two subunits in slightly different conformations as illustrated in Figure 6. The B10 Tyr33 residue is buried in the distal pocket. The phenolic oxygen atom of the B10 Tyr side chain forms an H-bond with the nitrogen atom of the side chain of Gln58 at the E11 position, which anchors the B helix to the E helix and creates a polar environment for the heme ligands, as shown in Figures 1 and 6. Resonance Raman spectroscopic results suggest that B10 Tyr33 forms H-bonds with various heme ligands, including CO and O_2 in the ferrous derivatives, and hydroxide in the ferric derivatives (*18*). The H-bonding interaction in the oxy derivative is confirmed by the crystallographic data, in which the phenolic hydroxide of B10 Tyr33 forms H-bonds with both oxygen atoms of the heme-bound dioxygen (Figure 1). On the basis of the Raman spectra of the NO derivative shown in Figure 2, B10 Tyr33 also forms an H-bond(s) with the heme-bound NO as illustrated in the inset of Figure 2. On the other hand, Tyr16 is located at the junction of the A and B helices. It introduces a sharp turn between the A and B helices by accepting an H-bond from the peptide amide group of His22. In subunit A, the phenolic hydroxide of Tyr16 also donates an H-bond to a nearby side chain group of Glu70 located at the end of the E helix, thereby providing stabilization energy for the B helix to dock against the E helix (Figure 6a). Interestingly, this H-bond is not present in the B subunit (Figure 6b). The origin of this structural heterogeneity is not clear. The H-bonding network surrounding Tyr16 in subunit B is illustrated in Figure 1. The third Tyr residue, Tyr72, is located in the pre-F helix loop on the proximal side of the heme, next to one of its two propionate groups. Its phenolic hydroxide forms an H-bond with the peptide backbone carbonyl group of Ala75, whose peptide amide group in turn

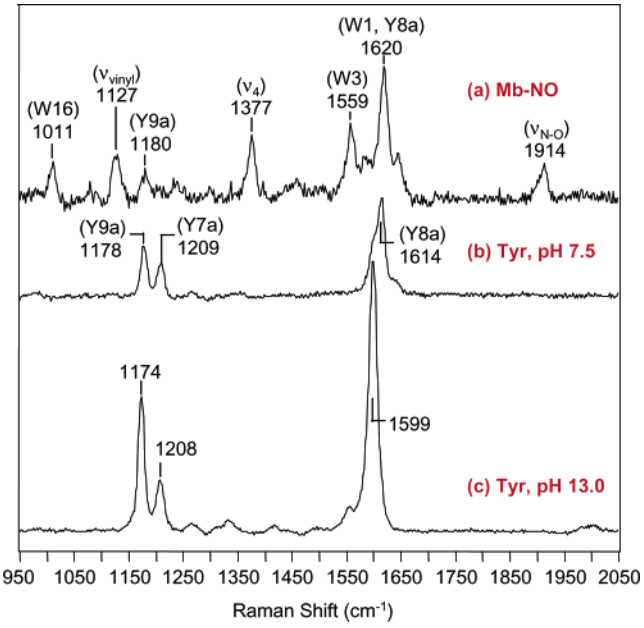

FIGURE 7: UV Raman spectra of the NO derivative of horse heart myoglobin (a), free Tyr in pH 7.5 buffer (b), and free Tyr in pH 13.0 buffer (c), with 244 nm excitation.

forms an H-bond with the propionate group of the heme. These interactions may provide part of the stabilization energy for the heme to anchor to the protein moiety in the heme pocket.

The Y_{8a} mode of Tyr is very sensitive to the electron density on its phenolic oxygen (*37*). Under neutral conditions, the Y_{8a} mode of Tyr in a free aqueous solution is identified at 1614 cm^{-1} (Figure 7b). When Tyr is deprotonated, it shifts to 1599 cm^{-1} because of the increase in the electron density in the phenolic oxygen (Figure 7c). On the other hand, it shifts to a higher frequency when the phenolic oxygen of Tyr forms an H-bond with a proton donor. The ferric heme of the aquo-met derivative of HbN is coordinated by a water molecule in the distal position at neutral pH (*18*). The Y_{8a} mode at 1616 cm^{-1} identified in the spectrum of the aquo-met derivative was assigned to B10 Tyr33 as discussed earlier (Figure 5a). It is 2 cm^{-1} higher than that of free Tyr in aqueous solution at neutral pH (Figure 7b), suggesting that the Tyr residue is, on average, in an environment with slightly positive electrostatic potential. This conclusion is consistent with the H-bonding interaction between B10 Tyr33 and E11 Gln58 as discussed earlier. On the other hand, the Y_{8a} mode at 1610 cm^{-1} was assigned to the Tyr72 residue that donates an H-bond to the peptide C═O group of the Ala residue at position 75 as illustrated in Figure 1. This H-bond draws the proton away from Tyr72 and increases its electron density that is reflected by the downshift of the frequency of the Y_{8a} mode. In contrast, the mode at 1624 cm^{-1} was assigned to the Tyr16 residue, which accepts an H-bond from the peptide NH_2 group of the His at position 22 that causes an upshift of the frequency, based on the structure of the B subunit of HbN shown in Figure 1.

After NO binds, the Y_{8a} mode of Tyr33 shifts from 1616 to 1622 cm^{-1} (Figure 5a,b). The 4 cm^{-1} upshift of the Y_{8a} mode suggests that the H-bond(s) between Tyr33 and the heme-bound NO strengthens the H-bond between Tyr33 and Gln58, thereby decreasing the electron density in the phenolic oxygen of the former residue. Likewise, the slight downshift of the Y_{8a} mode of Tyr72 from 1610 to 1608 cm^{-1} suggests that the H-bond between Tyr72 and Ala75 is strengthened. The most dramatic structural change occurs in the Tyr16 region, as reflected by the 15 cm^{-1} upshift of the Y_{8a} mode of the Tyr16 residue (Figure 5a,d). The upshift in frequency again suggests that the H-bond between Tyr16 and His22 is stronger in the NO-bound derivative.

The structural changes in the Tyr16 and Tyr72 region suggest that NO binding to the heme triggers a large-scale conformational change, because these residues are not local in the NO binding site. On the other hand, the change in the environment of B10 Tyr33 reflects the differences in the H-bonding network surrounding the heme-bound NO. Conformational changes induced by NO binding to the ferric heme have been reported for nitrophorin (*32*). Nitrophorin uses ferric heme to transport NO from the salivary gland of a blood-sucking insect to the victim, which results in vasodilation and a reduced level of blood coagulation (*6*). It was shown that nitrophorin has a widely open distal pocket in the absence of NO. Once NO binds to the heme iron, two flexible loops in the distal side pack around the NO and form a hydrophobic pocket (*32*). This conformational change introduces distortions to the heme group and causes the Fe−N−O structure to be bent. It was proposed that this unique heme environment stabilizes the NO and prevents autoreduction of the heme, which is very important for nitrophorin to perform its physiological function (*33*). Intriguingly, the Fe−NO stretching and Fe−N−O bending frequencies of nitrophorin determined by resonance Raman measurements were identical to those of the NO derivative of HbN (*38*), despite the fact that the distal pocket of nitrophorin is hydrophobic in contrast to the hydrophilic pocket of HbN (*18*, *19*). In contrast, horse heart myoglobin, which has a distal His at the E7 position that stabilizes the heme-bound NO, has a much more intense Fe−N−O bending mode with a lower frequency (572 cm^{-1}) and a higher Fe−NO stretching frequency (596 cm^{-1}) (*39*). The weakening of the Fe−N−O bending mode in HbN with the B10 Tyr → Phe mutation suggests that B10 Tyr influences the Fe−N−O geometry, possibly through H-bonding interactions.

In human hemoglobin, the allosteric structural transition induced by ligand binding to the heme is triggered by the movement of the heme iron, which is evident in the shift in the Fe−His stretching frequency from 229 to 214 cm^{-1} when the nanosecond photodissociated state relaxes to the equilibrium deoxy state (*40*, *41*). Intriguingly, the Fe−His stretching frequency of HbN is identical in the photodissociated state as compared to that of the equilibrium deoxy state (manuscript being prepared for publication), suggesting that the large-scale structural transition induced by NO binding to HbN is not initiated by the movement of the heme iron. The structural transition is also not triggered by the formation of the H-bonds between the B10 Tyr and the heme-bound NO, because if it was the case no structural changes in the Tyr16 and Tyr72 region would occur in the B10 Tyr → Phe mutant upon NO binding (spectrum a → d transition in Figure 5). The presence of the two structures in the oxy derivative of HbN demonstrates its structural plasticity; it also reveals a possible mechanism for the propagation of the protein structural changes from the NO binding site to the rest of the molecule. As highlighted in the crystallographic structures of the two subunits of HbN shown in

Figure 6, a significant structural difference occurs in the Tyr16 region, where the distance between Tyr16 and Glu70 increased from 2.74 Å in subunit A to 5.46 Å in subunit B. The breakage of the H-bond between Tyr16 and Glu70 in subunit B is accompanied by a tighter H-bonding network in the Tyr33 region, as indicated by a shorter Fe−O_2 bond and shorter distances among B10 Tyr, E11 Gln, and heme-bound O_2. These structural changes are also correlated with a slight distortion of the heme and significant conformational changes in its peripheral groups, which cause small changes in the H-bonding network in the Tyr72 region among the propionate group, Ala75, and Tyr72. It is plausible that NO binding to the heme iron introduces structural changes to the heme and its peripheral groups due to an electronic effect like that reported for nitrophorin (*33*, *38*, *42*, *43*), which subsequently affects the H-bonding network in the Tyr72 region. The changes in this pre-F helix loop region are transmitted to the B and E helices through the Tyr16 region to the distal Tyr33 region, because both Tyr16 and Tyr33 are involved in the H-bonding networks stitching the B and E helices together (see Figure 6). This structural transition causes Glu70 to move away from Tyr16, thereby strengthening the H-bond between Tyr16 and His22.

Previously, it was shown that the stabilization of dioxygen in HbN is a result of the H-bonding interactions between B10 Tyr and the heme-bound dioxygen as illustrated in Figure 1, based on resonance Raman and crystallographic data (*18*−*20*). Here we demonstrate that similar H-bonding interactions are present in the NO-bound ferric protein, causing the Fe−N−O moiety to be bent. In addition, NO binding to HbN triggers a novel large-scale structural transition. It is not clear whether the conformational change induced by NO binding in HbN plays any role in its physiological function. However, it provides an excellent model for understanding the ligand−protein interactions in heme proteins. In addition, the generation of large conformational changes by NO binding to heme may be a general property of ligand-induced regulation in many other heme proteins.

ACKNOWLEDGMENT

We thank Dr. Denis L. Rousseau for many valuable discussions.

REFERENCES

1. Cooper, C. E. (1999) *Biochim. Biophys. Acta 1411*, 290−309.
2. Wink, D. A., and Mitchell, J. B. (1998) *Free Radical Biol. Med. 25*, 434−456.
3. Fang, F. C. (1997) *J. Clin. Invest. 99*, 2818−2825.
4. Schmidt, H. H., and Walter, U. (1994) *Cell 78*, 919−925.
5. Ignarro, L. J. (1990) *Annu. Rev. Pharmacol. Toxicol. 30*, 535−560.
6. Ribeiro, J. M., Hazzard, J. M., Nussenzveig, R. H., Champagne, D. E., and Walker, F. A. (1993) *Science 260*, 539−541.
7. Andersen, J. F., Ding, X. D., Balfour, C., Shokhireva, T. K., Champagne, D. E., Walker, F. A., and Montfort, W. R. (2000) *Biochemistry 39*, 10118−10131.
8. Ignarro, L. J. (1992) *Biochem. Soc. Trans. 20*, 465−469.
9. Denninger, J. W., and Marletta, M. A. (1999) *Biochim. Biophys. Acta 1411*, 334−350.
10. Hobbs, A. J. (1997) *Trends Pharmacol. Sci. 18*, 484−491.
11. Feldman, P. L., Griffith, O. W., Hong, H., and Stuehr, D. J. (1993) *J. Med. Chem. 36*, 491−496.
12. Marletta, M. A. (1993) *J. Biol. Chem. 268*, 12231−12234.
13. Roman, L. J., Martasek, P., Miller, R. T., Harris, D. E., de La Garza, M. A., Shea, T. M., Kim, J. J., and Masters, B. S. (2000) *J. Biol. Chem. 275*, 29225−29232.
14. Zhao, Y., Brandish, P. E., Ballou, D. P., and Marletta, M. A. (1999) *Proc. Natl. Acad. Sci. U.S.A. 96*, 14753−14758.
15. Giardina, B., and Amiconi, G. (1981) *Methods Enzymol. 76*, 417−427.
16. Moore, E. G., and Gibson, Q. H. (1976) *J. Biol. Chem. 251*, 2788−2794.
17. Mukai, M., Savard, P. Y., Ouellet, H., Guertin, M., and Yeh, S. R. (2002) *Biochemistry 41*, 3897−3905.
18. Yeh, S. R., Couture, M., Ouellet, Y., Guertin, M., and Rousseau, D. L. (2000) *J. Biol. Chem. 275*, 1679−1684.
19. Couture, M., Yeh, S. R., Wittenberg, B. A., Wittenberg, J. B., Ouellet, Y., Rousseau, D. L., and Guertin, M. (1999) *Proc. Natl. Acad. Sci. U.S.A. 96*, 11223−11228.
20. Milani, M., Pesce, A., Ouellet, Y., Ascenzi, P., Guertin, M., and Bolognesi, M. (2001) *EMBO J. 20*, 3902−3909.
21. Ouellet, H., Ouellet, Y., Richard, C., Labarre, M., Wittenberg, B., Wittenberg, J., and Guertin, M. (2002) *Proc. Natl. Acad. Sci. U.S.A. 99*, 5902−5907.
22. Spiro, T. G. (1987) *Biological applications of Raman spectroscopy*, Wiley, New York.
23. Johnson, C. R., and Asher, S. A. (1984) *Anal. Chem. 56*, 2258−2261.
24. Rava, R. P., and Spiro, T. G. (1984) *J. Am. Chem. Soc. 106*, 4062−4064.
25. Kitagawa, T. (1992) *Prog. Biophys. Mol. Biol. 58*, 1−18.
26. Huang, S., Huang, J., Kloek, A. P., Goldberg, D. E., and Friedman, J. M. (1996) *J. Biol. Chem. 271*, 958−962.
27. Aki, M., Ogura, T., Shinzawa-Itoh, K., Yoshikawa, S., and Kitagawa, T. (2000) *J. Phys. Chem. B 104*, 10765−10774.
28. Tomita, T., Haruta, N., Aki, M., Kitagawa, T., and Ikeda-Saito, M. (2001) *J. Am. Chem. Soc. 123*, 2666−2667.
29. Spiro, T. G., and Kozlowski, P. M. (2001) *Acc. Chem. Res. 34*, 137−144.
30. Hu, S., and Kincaid, J. R. (1991) *J. Am. Chem. Soc. 113*, 2843−2850.
31. Hu, S., and Kincaid, J. R. (1993) *J. Biol. Chem. 268*, 6189−6193.
32. Weichsel, A., Andersen, J. F., Champagne, D. E., Walker, F. A., and Montfort, W. R. (1998) *Nat. Struct. Biol. 5*, 304−309.
33. Roberts, S. A., Weichsel, A., Qiu, Y., Shelnutt, J. A., Walker, F. A., and Montfort, W. R. (2001) *Biochemistry 40*, 11327−11337.
34. Asher, S. A. (1993) *Anal. Chem. 65*, 201A−210A.
35. Hashimoto, S., and Takeuchi, H. (1998) *J. Am. Chem. Soc. 120*, 11012−11013.
36. DeVito, V. L., Cai, M.-Z., Asher, S. A., Kehres, L. A., and Smith, K. M. (1992) *J. Phys. Chem. 96*, 6917−6922.
37. Rava, R. P., and Spiro, T. G. (1985) *J. Phys. Chem. 89*, 1856−1861.
38. Maes, E. M., Walker, F. A., Montfort, W. R., and Czernuszewicz, R. S. (2001) *J. Am. Chem. Soc. 123*, 11664−11672.
39. Tomita, A., Hirota, S., Ogura, T., Olson, J. S., and Kitagawa, T. (1999) *J. Phys. Chem. B 103*, 7044−7054.
40. Nagai, K., and Kitagawa, T. (1980) *Proc. Natl. Acad. Sci. U.S.A. 77*, 2033−2037.
41. Friedman, J. M., Rousseau, D. L., Ondrias, M. R., and Stepnoski, R. A. (1982) *Science 218*, 1244−1246.
42. Weichsel, A., Andersen, J. F., Roberts, S. A., and Montfort, W. R. (2000) *Nat. Struct. Biol. 7*, 551−554.
43. Wondimagegn, T., and Ghosh, A. (2001) *J. Am. Chem. Soc. 123*, 5680−5683.

BI035798O